Factors governing the electrochemical synthesis of α-nickel (II) hydroxide

R. S. JAYASHREE and P. VISHNU KAMATH*
Department of Chemistry, Central College, Bangalore University, Bangalore 560001, India
*(*author for correspondence)*

Abstract

The electrodeposition of α-nickel hydroxide is promoted by the simultaneous chemical corrosion of the electrode by an acidic nitrate bath. Chemical corrosion results in the formation of a poorly ordered layered phase which is structurally similar to α-nickel hydroxide and provides nucleation sites for the deposition of the latter. Therefore under conditions which enhance corrosion rates such as low current density ($< 1.3 \, \mathrm{mA \, cm^{-2}}$), high temperature (60 °C), high nickel nitrate concentration ($\geqslant 1 \, \mathrm{M}$) and the resultant low pH (~ 1.7), α-nickel hydroxide electrodeposition is observed, while β-nickel hydroxide forms under other conditions. Further, α-nickel hydroxide deposition is more facile on an iron electrode compared to nickel or platinum.

1. Introduction

Nickel hydroxide, which is the cathode material of all nickel based alkaline secondary cells, exists in two polymorphic modifications known as α and β [1]. The α form of nickel hydroxide has a higher reversible discharge capacity compared to the β form as a result of which the synthesis and stabilization of α-nickel hydroxide [2–4] is a subject of great interest to battery technologists. Of the many synthetic routes [5–7] to α-nickel hydroxide, the electrochemical route [8–11] by the cathodic reduction of a nickel nitrate solution is the most widely employed. As the outcome of an electrochemical reaction depends upon a number of parameters such as current density, choice of the electrode, the concentration, composition and pH of the electrolyte, the temperature of deposition and the mode of electrolysis (whether potentiostatic or galvanostatic), there have been a number of studies which have examined the effect of these parameters on the electrosynthesis of nickel hydroxide, both inside plaques and at plane electrodes. Most significant among these, has been the work of Weidner and coworkers [12–14] who have employed in situ experimental techniques, as well as theory, to understand the electrochemical deposition of nickel hydroxide. They have quantified the growth of the nickel hydroxide deposit as a function of various electrodeposition parameters [14]. In all these investiga-

tions, the deposit has been assumed to be β-nickel hydroxide (molecular weight, $93 \, \mathrm{g \, mol^{-1}}$). However, recent work [11, 15, 16] has shown that under a number of conditions, the electrodeposited hydroxide is of the α-variety with a composition $\mathrm{Ni(OH)_{2-x}(A^{n-})_{x/n} z H_2 O}$ ($x \sim 0.15$; $z = 0.66 - 1$; $\mathrm{A^{n-} = Cl^-, \, NO_3^-, \, SO_4^{2-}}$; calculated molecular weight, $107 - 117 \, \mathrm{g \, mol^{-1}}$). In the present work the molecular weight is in the range $116 - 122 \, \mathrm{g \, mol^{-1}}$. In the light of these studies it is important to understand the factors governing the electrochemical synthesis of α-nickel hydroxide, as distinct from β-nickel hydroxide, so that quantitative models correctly reflect the reactions taking place at the electrode. In this work we investigate the factors governing the electrosynthesis of α-nickel hydroxide.

2. Experimental details

2.1. *Synthesis*

All nickel hydroxide samples were prepared by cathodic reduction of nickel nitrate solutions (concentration $0.25 - 1 \, \mathrm{M}$) galvanostatically (current density, $1.3 - 20 \, \mathrm{mAcm^{-2}}$) in a divided cell using platinum, nickel or iron electrodes. A potassium nitrate solution of the same concentration as that of the nickel nitrate solution was used in the anodic chamber and platinum was used as

counter electrode. The deposition was carried out for 7 − 23 h, during which no ageing of the nickel hydroxide was observed. The deposition was carried out at different temperatures using a thermostat controlled waterbath. During electrodeposition the potential of the working electrode was monitored using a high impedence Meco (India) voltmeter and a SCE reference. The precipitate formed in the cathode chamber was filtered, washed in distilled water and dried to constant weight at 65 °C.

Corrosion products of nickel and iron electrodes were obtained after prolonged (45 − 140 h) dipping of the electrodes in a 1 M nickel nitrate solution (pH 1.7). To estimate the extent of corrosion taking place simultaneously with electrodeposition, sintered nickel porous plaques (porosity 80%, geometric area 8 cm^2) were cathodically polarised in a 2 M potassium nitrate solution acidified to the same pH as that of the 1 M nickel nitrate solution in an undivided cell using two plane platinum counters. To eliminate the effect of chemical corrosion during soaking [17], the electrodes were dipped and withdrawn from the electrolyte under 'power on' conditions. The plaques were weighed before and after the polarization experiments.

2.2. Physical characterization

All metal hydroxide samples were characterized by powder X-ray diffractometry (Jeol model JDX8P powder diffractometer, Cu$K\alpha$ radiation) and infrared spectroscopy (Nicolet model Impact 400D FTIR spectrometer, KBr pellets, 3 cm^{-1} resolution). Thermogravimetry (TG) data were acquired on a home-made system (heating rate 2.5 °C min^{-1}).

2.3. Wet chemical analysis

The nickel content of the hydroxide was determined by gravimetry. The hydroxyl content was determined by dissolving an accurately weighed amount of hydroxide in excess acid and back titrating the excess against a standard base using a pH meter. The hydroxyl content was found to be substoichiometric in α-nickel hydroxide. The hydroxyl deficiency was compensated by the inclusion of nitrate ions for charge neutrality. The unaccounted weight was attributed to water in order to obtain an approximate formula which was found to match with the TG results within acceptable limits of accuracy.

3. Results and discussion

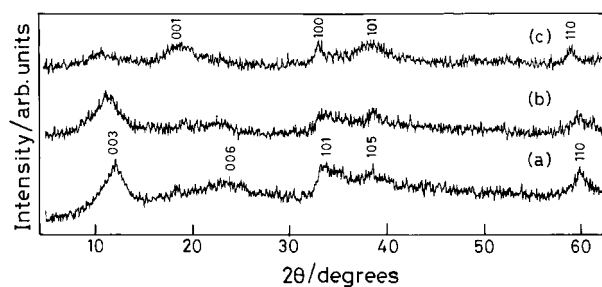Figure 1 shows the powder X-ray diffraction (XRD) patterns of nickel hydroxide samples obtained by the electroreduction of a 1 M nickel nitrate solution using a nickel electrode at various current densities. The prominent d spacings are listed in Table 1. It is evident that at low current densities the product is the α-hydroxide, as evidenced by the appearance of a low angle reflection at about 7.4 Å followed by another at about 3.7 Å. The asymmetry on the higher 2θ side in the reflections observed in the 2.6 − 2.3 Å range is characteristic of the turbostratic disorder manifest in α-nickel hydroxide. At higher current densities (>20 mA cm^{-2}), the 7.4 Å reflection becomes weak and the (0 0 1) reflection of β-nickel hydroxide appears at 4.6 Å, which indicates that the product is predominantly β-nickel hydroxide. At the same time, the peak shapes change in the 2.7 − 2.3 Å range indicating the formation of a more ordered structure. As can be seen from Figure 2, the quality of the α-nickel hydroxide deteriorates even at low current densities when the nickel nitrate concentration is reduced to 0.25 M. This difference may arise either due to (i) the reduced concentration of Ni^{2+} ions or (ii) by the higher pH of the diluted electrolyte. But when 0.25 M nickel nitrate solution was acidified by the addition of nitric acid to the same pH as that of 1 M

Fig. 1. Powder XRD patterns of nickel hydroxide samples obtained from 1 M nickel nitrate solutions at 1.29 (a), 2.56 (b) and 20 mA cm^{-2} (c) current densities, respectively.

Table 1. Powder X-ray diffraction data of nickel hydroxide samples obtained from a 1 M nickel nitrate solution using different electrodes

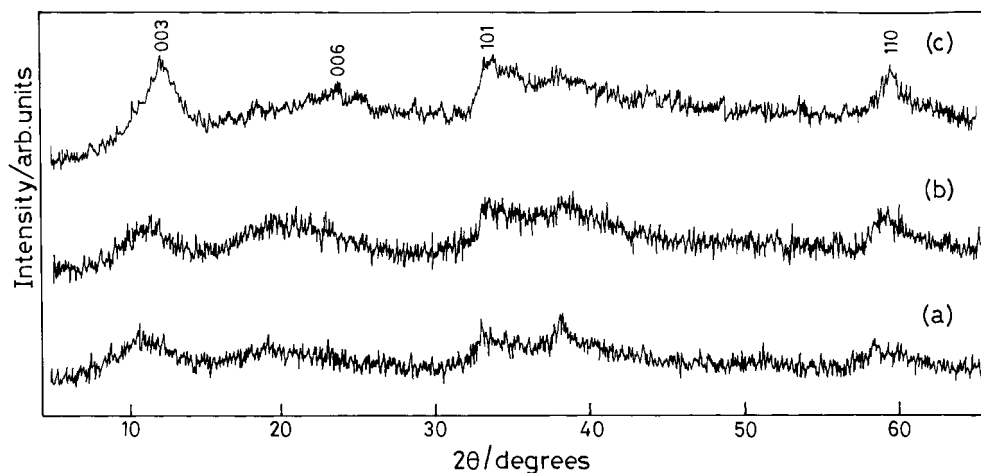| h k l	d/Å			
	Ni electrode (RT)	Ni electrode (60 °C)	Pt electrode (RT)	Fe electrode (RT)
0 0 3	7.38	7.08	7.53	7.31
0 0 6	3.75	3.53	–	3.66
1 0 1	2.65	2.66	–	2.66
1 0 2	–	–	2.61	–
1 0 3	–	2.51	–	–
1 0 5	–	–	2.30	–
1 1 0	1.54	1.54	1.55	1.55
a/Å	3.09	3.09	3.09	3.09
c/Å	22.36	21.24	22.49	21.93

RT: room temperature synthesis

Fig. 2. Powder XRD patterns of nickel hydroxide samples obtained using a nickel electrode from 0.25 M (a), acidified 0.25 M (b) and 1 M (c) nickel nitrate solutions, respectively.

nickel nitrate, the crystallinity of the α-nickel hydroxide did not improve, showing that the former factor is more important.

On the one hand, the crystallinity of the α-nickel hydroxide electrodeposited at elevated temperature (60 °C) is much superior to that obtained at room temperature (26 – 28 °C) from 1 M nickel nitrate solution. On the other hand, a dilute electrolyte yields β-nickel hydroxide at elevated temperature (Figure 3).

From these observations, it is evident that the electrodeposition of α-nickel hydroxide is promoted at low current densities, high nickel nitrate concentrations and at elevated temperature. These conditions also promote the aggressive corrosion of nickel electrodes soaked in a nickel nitrate solution [17]. It appears that conditions promoting aggressive corrosion of the electrode also promote the electrodeposition of α-nickel

hydroxide. To verify this hypothesis, nickel hydroxide was electrodeposited at a mild steel electrode, expected to be the most susceptible to corrosion, and the resultant product was compared with that obtained at a platinum electrode (Figure 4). It is at once evident that mild steel electrodes yield the most crystalline α-nickel hydroxide samples, while platinum yields a poorly crystalline phase.

The nickel hydroxides electrodeposited at nickel, mild steel and platinum electrodes were chemically analysed and the results are given in Table 2. The iron content of the α-nickel hydroxide obtained at mild steel is only 0.07% and at this low concentration Fe^{3+} is not expected to affect the structure or morphology of the hydroxides.

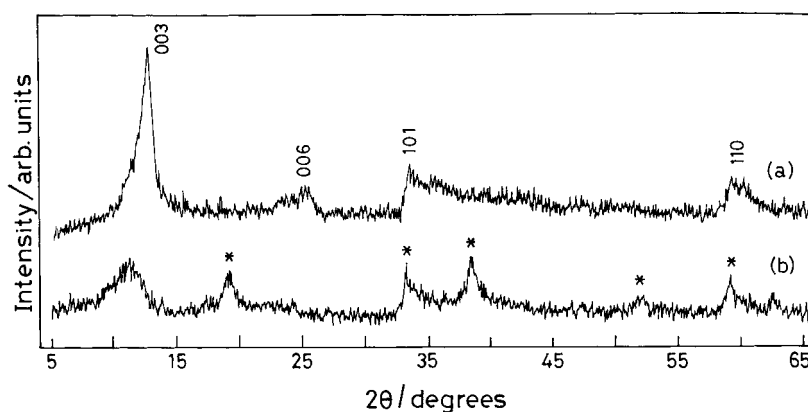To understand better this phenomenon, nickel and mild steel plates were kept soaking in a 1 M nickel nitrate

Fig. 3. Powder XRD patterns of nickel hydroxide samples obtained using a nickel electrode at 60 °C from 1 M (a) and 0.25 M (b) nickel nitrate solutions, respectively. Features marked by the asterisk are due to β-nickel hydroxide.
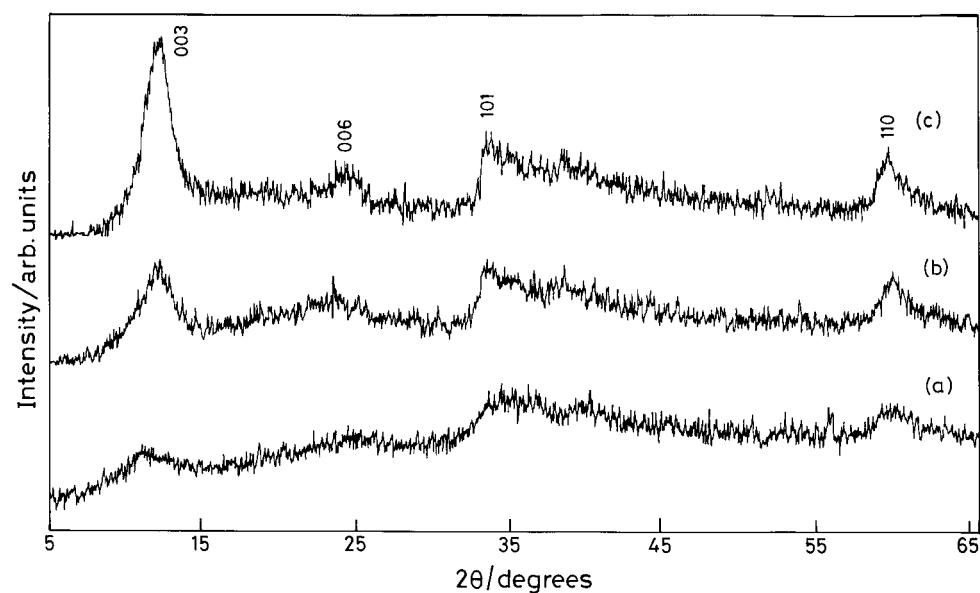
Fig. 4. Powder XRD patterns of nickel hydroxide samples obtained from a 1 M nickel nitrate solution using Pt (a), Ni (b) and mild steel (c) electrodes, respectively.

solution for $45 - 140$ h. Scaly corrosion products were deposited on the nickel plate, while a yellow–green precipitate was found to form in copious quantities around the mild steel plate. Figure 5 shows the powder XRD of the corrosion product of nickel and the prominent d spacings are listed in Table 3. The powder XRD patterns of the corrosion products of nickel and mild steel could be indexed on a hexagonal cell ($a = 3.08$ Å, $c = 24.3$ Å and $a = 3.09$ Å, $c = 23.7$ Å, respectively) similar to that of α-nickel hydroxide. In Figure 6 the infrared spectrum of the corrosion product is compared with that of the α-hydroxide. Both spectra have common features which include (i) a broad peak centred around 3400 cm^{-1} corresponding to a hydrogen bonded OH vibration, (ii) absorptions at $1000-1500$ cm^{-1} due to intercalated anions and (iii) absorptions at 640 and 470 cm^{-1} due to the Ni–O–H bending and Ni–O streching vibrations, respectively.

It is, however, widely assumed that nickel electrodes do not undergo corrosion during the electrodeposition of nickel hydroxide, as hydrogen evolved during cathodic polarization, provides a protective blanket. To verify this assumption, nickel plaques were cathodically polarized in 2 M potassium nitrate solution acidified to the same pH as that of a 1 M nickel nitrate solution. The weight loss suffered by the plaques simultaneously with cathodic polarization is given in Table 4. While the extent of corrosion is much less than that observed during dipping [17], it is nevertheless nonzero, showing that minute levels of corrosion take place simultaneously with cathodic polarization, especially at low current densities. This is understandable as hydrogen evolution at low current densities is not adequate to provide the protective blanket to suppress corrosion. The corrosion sites then act as nuclei facilitating the electrodeposition of α-nickel hydroxide. The effect is more pronounced in the case of sintered nickel porous plaques, whose actual surface area is many times more than the geometric area and, consequently, the true current density is much lower than that evaluated on the basis of the geometric area.

Table 2. Chemical composition of α-nickel hydroxide samples obtained by electrosynthesis (ES) using different electrodes

Electrodes used for ES	Approximate formulae[a]	Total weight loss / %	
		Expected	Observed[b]
Platinum	Ni(OH)$_{1.76}$(NO$_3$)$_{0.24}$·1.02 H$_2$O	38.72	38.70
Nickel	Ni(OH)$_{1.77}$(NO$_3$)$_{0.23}$·0.73 H$_2$O	35.59	35.0
Mild steel	Ni(OH)$_{1.77}$(NO$_3$)$_{0.23}$·0.73 H$_2$O	35.59	35.10

[a] As obtained from wet chemical analysis
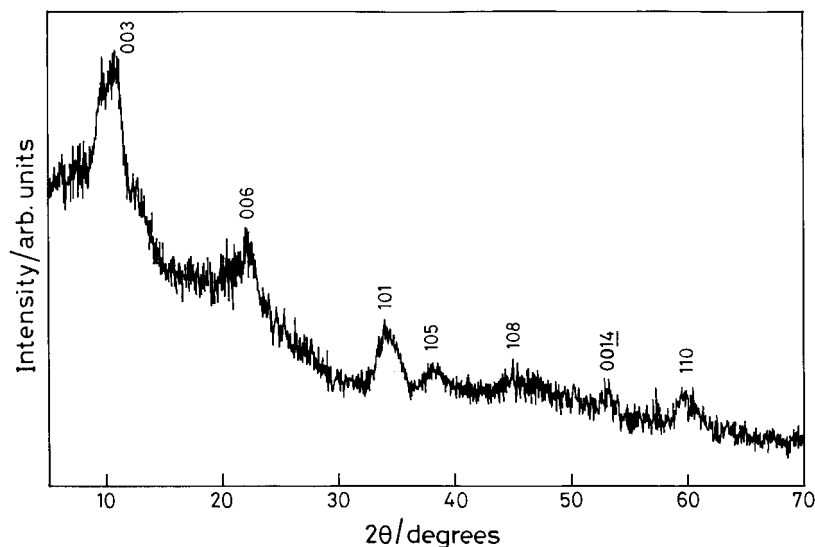[b] From TG data

Fig. 5. Powder XRD pattern of the corrosion product of a nickel electrode in a 1 M nickel nitrate solution.
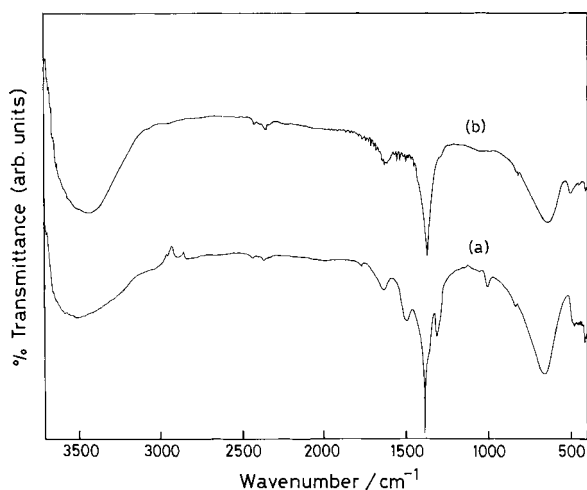

Fig. 6. Infrared spectra of α-nickel hydroxide (a) and the corrosion product of nickel (b).

At higher current densities, no corrosion of either plane electrodes or plaques was observed probably due to the protective hydrogen blanket. Under these conditions, copious precipitation of β-nickel hydroxide was observed.

In conclusion, electrodeposition of α-nickel hydroxide is promoted at low current densities, high nickel nitrate concentrations, low pH and elevated temperatures at electrodes that are susceptible to chemical corrosion. This study paves the way for the synthesis of α-hydroxides in other systems where polymorphism is not known to exist.

Table 3. Powder X-ray diffraction data for the corrosion products of nickel and mild steel in a 1 M nickel nitrate solution

h k l	$d/\text{Å}$	
	Nickel	Mild Steel
0 0 3	8.14	7.91
0 0 6	4.08	3.95
1 0 1	2.64	–
1 0 2	–	2.62
1 0 5	2.37	2.33
1 0 8	2.00	1.97
0 0 14	1.73	–
1 1 0	1.55	1.54
1 1 3	–	1.52
0 0 18	1.35	–
$a/\text{Å}$	3.08	3.09
$c/\text{Å}$	24.3	23.7

Table 4. Weight loss suffered by sintered Ni porous plaques during cathodic polarization in a potassium nitrate solution of pH 1.5

Current density $/\text{mA cm}^{-2}$	Weight loss $/\text{mg}\,(\text{g Ni})^{-1}\,\text{h}^{-1}$
2	0.13
1.5	0.61
1	17.34

454

References

1. P. Oliva, J. Leonardi, J.F. Laurent, C. Delmas, J.J. Braconnier, M. Figlarz and F. Fievet, *J. Power Sources* **8** (1982) 229.
2. J.J. Braconnier, C. Delmas, C. Fouassier, M. Figlarz, B. Beaudouin and P. Hagenmuller, *Rev. Chim. Min.* **21** (1984) 496.
3. C. Faure, C. Delmas and P. Willmann, *J. Power Sources* **36** (1991) 497.
4. P.V. Kamath, M. Dixit, L. Indira, A.K. Shukla, V.G. Kumar and N. Munichandraiah, *J. Electrochem. Soc.* **141** (1994) 2956.
5. C. Faure, C. Delmas and M. Fouassier, *J. Power Sources* **35** (1991) 279.
6. S. LeBihan, J. Guenot and M. Figlarz, *C.R. Acad. Sci., Ser. C.* **270** (1970) 2131.
7. P.V. Kamath, J. Ismail, M.F. Ahmed, G.N. Subbanna and J. Gopalakrishnan, *J. Mater. Chem.* **3** (1993) 1285.
8. E.J. McHenry, *Electrochem. Technol.* **5** (1967) 275.
9. K.C. Ho, *J. Electrochem. Soc.* **134** (1987) 52C.
10. K.C. Ho and J. Jorne, *J. Electrochem. Soc.* **137** (1990) 149.
11. F. Portemer, A. Delahaye-Vidal and M. Figlarz, *J. Electrochem. Soc.* **139** (1992) 671.
12. C.C. Streinz, A.P. Hartman, S. Motupally and J.W. Weidner, *J. Electrochem. Soc.* **142** (1995) 1084.
13. S. Motupally, C.C. Streinz and J.W. Weidner, *J. Electrochem. Soc.* **142** (1995) 1401.
14. M. Murthy, G.S. Nagarajan, J.W. Weidner and J.W. Van Zee, *J. Electrochem. Soc.* **143** (1996) 2319.
15. M. Wohlfahrt-Mehrens, R. Oesten, P. Wilde and R.A. Huggins, *Solid State Ionics* **86–88** (1996) 841.
16. G.H.A. Therese and P.V. Kamath, *J. Appl. Electrochem.* **28** (1998) 539.
17. C.E. Baumgartner, *J. Electrochem. Soc.* **135** (1988) 36.